THE ASTROPHYSICAL JOURNAL, 492:L107–L110, 1998 January 10
© 1998. The American Astronomical Society. All rights reserved. Printed in U.S.A.

# NICMOS IMAGING OF THE NUCLEI OF ARP 220

N. Z. SCOVILLE AND A. S. EVANS
California Institute of Technology, Pasadena, CA 91125
N. DINSHAW
Lick Observatory, University of California Observatories, University of California, Santa Cruz, Santa Cruz, CA 95064
R. THOMPSON, M. RIEKE, G. SCHNEIDER, F. J. LOW, D. HINES, AND B. STOBIE
Steward Observatory, University of Arizona, Tucson, AZ 85721
E. BECKLIN
University of California, Los Angeles, CA 90095
AND
H. EPPS
Lick Observatory, University of California Observatories, University of California, Santa Cruz, Santa Cruz, CA 95064
*Received 1997 July 29; accepted 1997 October 30; published 1997 December 30*

## ABSTRACT

We report high-resolution imaging of the ultraluminous infrared galaxy Arp 220 at 1.1, 1.6, and 2.22 $\mu$m with the Near-Infrared Camera and Multiobject Spectrometer on the *Hubble Space Telescope*. The diffraction-limited images at 0.″1–0.″2 resolution clearly resolve both nuclei of the merging galaxy system and reveal for the first time a number of luminous star clusters in the circumnuclear envelope. The morphologies of both nuclei are strongly affected by dust obscuration, even at 2.2 $\mu$m: the primary nucleus (west) presents a crescent shape, concave to the south, and the secondary (eastern) nucleus is bifurcated by a dust lane with the southern component being very reddened. In the western nucleus, the morphology of the 2.2 $\mu$m emission is most likely the result of obscuration by an opaque disk *embedded* in the nuclear star cluster. The morphology of the central starburst cluster in the western nucleus is consistent with either a circumnuclear ring of star formation or a spherical cluster with the bottom half obscured by the embedded dust disk. Comparison of centimeter-wave radio continuum maps with the near-infrared images suggests that the radio nuclei lie in the dust disk on the west and near the highly reddened southern component of the eastern complex. The radio nuclei are separated by 0.″98 (corresponding to 364 pc at 77 Mpc), and the half-widths of the infrared nuclei are ~0.″2–0.″5. At least eight unresolved infrared sources—probably globular clusters—are also seen in the circumnuclear envelope at radii of 2″–7″. Their near-infrared colors do not significantly constrain their ages.

*Subject headings:* galaxies: active — galaxies: individual (Arp 220)

## 1. INTRODUCTION

Arp 220 (IC 4553/4), with an infrared luminosity of $1.5 \times 10^{12}\ L_\odot$ at $\lambda = 8$–$1000$ $\mu$m, is one of the nearest ultraluminous infrared galaxies (Soifer et al. 1987). Visual wavelength images reveal two faint tidal tails, indicating a recent tidal interaction (cf. Joseph & Wright 1985), and high-resolution ground-based radio and near-infrared imaging show a double nucleus (Baan et al. 1987; Graham et al. 1990). The radio nuclei are separated by 0.″98 at P.A. ~ 90° (Baan & Haschick 1995). The system is also extraordinarily rich in molecular gas ($M_{\rm H_2} \sim 9 \times 10^9\ M_\odot$; Scoville, Yun, & Bryant 1997), and about $\frac{2}{3}$ of this gas and dust is concentrated in a thin disk with radii of $\leq$250 pc. Ground-based observations at 10–30 $\mu$m suggest that the far-infrared luminosity originates from a region of similar size (Wynn-Williams & Becklin 1993). To power the energy output seen in the infrared by young stars requires a star formation rate of $\sim 10^2\ M_\odot\ {\rm yr}^{-1}$. Alternatively, if the luminosity originates from an active galactic nucleus, this source must be sufficiently obscured by dust that even the mid-infrared emission lines are highly extinguished since spectroscopy with the *Infrared Space Observatory* shows no evidence of very high ionization lines at wavelengths out to 40 $\mu$m (Sturm et al. 1996).

In this Letter we report near-infrared imaging at $\lambda = 1$–$2.2$ $\mu$m with 0.″1–0.″2 resolution obtained using the Near-Infrared Camera and Multiobject Spectrometer (NICMOS) camera on the *Hubble Space Telescope* (*HST*). These high-resolution data clearly reveal the complex nature of the nuclei with the morphologies of both near-infrared nuclei strongly affected by dust obscuration and enable an improved registration of the infrared relative to the radio nuclei. Throughout this Letter, we adopt a distance of 77 Mpc (1″ corresponds to 373 pc) for Arp 220 using $H_0 = 75$ km s$^{-1}$ Mpc$^{-1}$ (Soifer et al. 1987).

## 2. OBSERVATIONS AND RESULTS

Arp 220 was observed with NICMOS camera 2 on the *HST* 1997 April 4 as part of the Early Release Observations (ERO) program. Camera 2 has a 256 × 256 HgCdTe array with 0.″076 pixels, providing a 19.″2 field of view. Images were obtained in the F110W, F160W, and F222M filters, providing resolutions of 0.″11, 0.″16, and 0.″22, respectively. For both the galaxy and a *HST* guide star, observed to determine the point-spread function, a four-step dither pattern was executed with offsets of 5.4 pixels (0.″41). At each position in the dither pattern on Arp 220, two integrations, each lasting 128 s, with multiple nondestructive reads (MULTIACCUM) were obtained. The data were dark-subtracted, flat-fielded, and corrected for cosmic rays with the IRAF software NICMOS pipeline routines. The dithered images were shifted and co-added using the drizzle routine in IRAF. The flux scale employed calibration factors of $2.35 \times 10^{-6}$, $2.77 \times 10^{-6}$, and $6.11 \times 10^{-6}$ Jy (ADU s$^{-1}$)$^{-1}$ at 1.1, 1.6, and 2.22 $\mu$m (Rieke et al. 1997). The measured fluxes at $H$ (1.6 $\mu$m) and $K$ (2.22 $\mu$m) for the nuclear sources and for a 5″ aperture agree to better than 10% with those obtained from ground-based imaging by Carico et al. (1990).

TABLE 1
SOURCE PROPERTIES

| | $\Delta\alpha$[a] | $\Delta\delta$[a] | $m_{1.1}$[b] | $m_{1.25}$[c] | $m_{1.6}$[b] | $m_{2.2}$[b] | $m_{1.25-1.6}$ | $m_{1.6-2.2}$ | FWHM (arcsec) | Aperture (arcsec) |
|---|---|---|---|---|---|---|---|---|---|---|
| Component | | | | | | | | | | |
| W ..... | 0.00 | 0.00 | 16.29 | 15.40 | 14.10 | 13.04 | 1.30 | 1.06 | 0.49 × 0.22 | 0.92 × 0.58 |
| S ..... | E 0.21 | −0.65 | 18.00 | 17.28 | 16.09 | 15.16 | 1.19 | 0.93 | 0.26 × 0.19 | 0.40 × 0.40 |
| SE ..... | E 1.00 | −0.33 | 18.70 | 17.68 | 16.31 | 14.83 | 1.37 | 1.48 | 0.26 × 0.23 | 0.40 × 0.40 |
| NE ..... | E 1.13 | 0.07 | 17.47 | 16.57 | 15.27 | 14.14 | 1.30 | 1.13 | 0.34 × 0.26 | 0.55 × 0.55 |
| All sources ..... | E 0.57 | −0.24 | 13.72 | 13.08 | 11.95 | 11.13 | 1.13 | 0.82 | ... | 5 circular |
| Clusters | | | | | | | | | | |
| 1 ..... | W 1.47 | −4.80 | 20.50 | 20.15 | 19.34 | 19.12 | 0.81 | 0.22 | ... | ... |
| 2 ..... | E 4.76 | −2.36 | 21.35 | 21.03 | 20.25 | 20.21 | 0.78 | 0.04 | ... | ... |
| 3 ..... | W 0.63 | −2.35 | 21.71 | 21.16 | 20.11 | ... | 1.05 | ... | ... | ... |
| 4 ..... | W 5.17 | 4.56 | 21.81 | 21.56 | 20.89 | ... | 0.66 | ... | ... | ... |
| 5 ..... | E 1.29 | −4.46 | 22.14 | 21.70 | 20.77 | 20.70 | 0.93 | 0.07 | ... | ... |
| 6 ..... | E 3.83 | −1.06 | 22.48 | 22.19 | 21.47 | ... | 0.72 | ... | ... | ... |
| 7 ..... | W 0.58 | 4.74 | 22.87 | 22.52 | 21.71 | ... | 0.81 | ... | ... | ... |
| 8 ..... | E 7.11 | 1.83 | 22.89 | 22.32 | 21.25 | ... | 1.07 | ... | ... | ... |

[a] Offsets are in arcseconds relative to the peak at 2.2 $\mu$m, $\alpha_{1950} = 15^h32^m46\overset{s}{.}90$, $\delta_{1950} = +23°40'07\overset{''}{.}94$, based on the registration of the infrared and radio as discussed in the text.

[b] Magnitudes are based on the flux calibration of Rieke et al. 1997 and have a typical uncertainty of $\pm 0.1$ mag; $m = 0$ corresponds to 1922, 1075, and 667 Jy at 1.1, 1.6, and 2.22 $\mu$m.

[c] Magnitudes are interpolated from $m_{1.1}$ and $m_{1.6}$ magnitudes.

At 1.1 $\mu$m, a direct comparison is not possible since the standard *J* filter is at 1.25 $\mu$m. The rms noise levels in the final images are 12, 15, and 35 $\mu$Jy arcsec$^{-2}$ at 1.1, 1.6, and 2.22 $\mu$m, respectively.

For observations with NICMOS camera 2, the angular resolutions are a factor of 2 lower at 2.22 $\mu$m than at 1.1 $\mu$m. This can seriously hinder attempts to analyze color gradients where there are compact emission sources unless the images at each wavelength are convolved or deconvolved to a common resolution. We have adopted two approaches: convolving the two short wavelength images to the resolution of the raw image at 2.22 $\mu$m and deconvolving the two long wavelength images to the resolution at 1.1 $\mu$m. The former is, of course, the safest approach but provides more limited spatial resolution. For the latter approach, deconvolution was done with the Richardson-Lucy algorithm without damping (Busko & Stobie 1997) to achieve 0.″14 resolution.

In Figure 1 (Plate L8) the images for the entire camera 2 field from the three bands are combined in false color. The image clearly reveals the structure around the twin nuclei separated by ~1″ east-west in addition to extended emission from the system out to ≥8″. At least eight unresolved (≤30 pc) sources are also seen at radii of 2–7″—the brightest being approximately 5″ southwest of the nucleus. All of them have bluer colors than the nuclei, but their magnitudes are sufficiently bright that they cannot be individual stars. We hereafter refer to them as clusters. The brightest of these clusters (1, 2, and 4) are seen in the visible band *HST* imaging of Shaya et al. (1994), and they are also clearly seen in subsequent *I*-band *HST* imaging (Borne & Lucas 1997).

The central region is shown in contour form in Figures 2, 3, and 4 (Plates L9, L10, and L11) using the original drizzled images at each wavelength, images convolved to 0.″22 resolution, and images deconvolved to 0.″11 resolution, respectively. In each case, the lower right-hand panel shows the ratio of the 2.22/1.1$\mu$m data. Coordinate offsets in Figures 2–4 are measured from the peak of the deconvolved 2.22 $\mu$m emission in the west nucleus. Flux measurements for the nuclear components and all identified cluster sources are listed in Table 1 along with measured sizes (FWHM) for resolved structures.

## 3. ANALYSIS AND DISCUSSION

Most of the near-infrared emission from the nuclear region of Arp 220 must be stellar (rather than hot dust or shock-excited emission lines) since the strength of the CO overtone absorption at 2.35 $\mu$m requires that ≥90% of the observed near-infrared flux in a 5″ aperture arises from stars (Armus et al. 1995; Shier, Rieke, & Rieke 1996). In previous ground-based images (e.g., Graham et al. 1990), the core of Arp 220 appears as two nuclei separated east-west by 0.″95. In the *HST* NICMOS images, the eastern nucleus breaks up into northern (NE) and southern (SE) components separated by 0.″4—the latter appears highly reddened and is barely visible in the 1.1 $\mu$m image. And the bright nucleus on the west (W), is seen as a *crescent* arc in the new images. Thus, for both nuclei, their morphology, even at $\lambda$ = 2.2 $\mu$m (where the extinction is 10 times less than $A_V$) appears strongly influenced by dust extinction. In addition, a new component is seen ~0.″6 south of the western nucleus (S) and another midway between the two nuclei.

### 3.1. *Registration*

The accuracy of the guide star position for the Arp 220 observations was insufficient to independently determine the absolute positions of the near infrared images. We have therefore registered the infrared images by comparison with centimeter-wave radio continuum maps for which the coordinates are well determined. Graham et al. (1990) matched the brightest radio sources (A and B; Baan & Haschick 1995) with the brightest portions of the eastern and western nuclei (i.e., components NE and W). However, this placement now seems unlikely since the separation and position angles of the two radio components and the two brightest infrared components are significantly different. Instead, we suggest that both of the two brightest radio components are located within the areas of very high extinction—south of the W component and between the NE and SE sources. This registration places the weak radio source C precisely on the southern (S) infrared source, which is relatively blue and therefore unlikely to be strongly extincted. Using the 2.22/1.1 $\mu$m ratio image (Fig. 3) to estimate the relative extinction across the region, we have crudely corrected

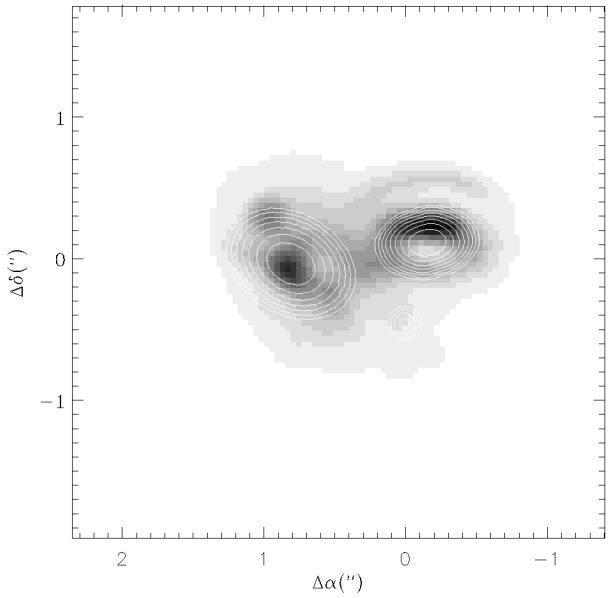


FIG. 5.—Radio continuum sources at 6 cm are superposed as contours on the extinction-corrected 2.22 $\mu$m image (see text). The radio source structure is derived from the deconvolved source sizes and position angles given by Baan & Haschick (1995). The registration of the radio and infrared is discussed in the text. The weak radio component C coincides with the infrared source S, which is not apparent in the corrected 2.22 $\mu$m image because of its low extinction, i.e., relatively blue color. The coordinates are offsets from the peak at 2.22 $\mu$m ($\alpha_{1950}$= 15$^h$32$^m$46$^s$.90, $\delta_{1950}$= +23°40′07″.94).

the 2.22 $\mu$m image for extinction under the assumption that the dust is in the foreground, i.e., not mixed with the stars. In Figure 5, the radio source contours from Baan & Haschick (1995) are shown superposed on this "extinction-corrected" 2.22 $\mu$m image using the registration discussed above. Radio source B lies within the dark area below the crescent on the W source, while A is at the north of the reddened SE infrared source. Support for our registration of the near-infrared emission is provided by the strong morphological similarity of the infrared structure shown here and the $H_2CO$ emission (Baan & Haschick 1995)—the latter exhibits similar offsets relative to the radio continuum.

### 3.2. *Reddening*

The 2.22/1.1 $\mu$m ratio images in Figures 2–4 may be used to probe variations in the extinction, assuming that the intrinsic color of the underlying stars is not strongly varying. The false color image for the deconvolved data (Fig. 1) clearly shows an overall increase in the reddening toward the central regions of Arp 220—in the annulus at 2″–4″ radii, $m_{1.1-2.2}$ = 1.79 mag, while inside the 2″ radius, $m_{1.1-2.2}$ = 2.75 mag. In the central 2″, Figure 3 reveals even larger variations: high reddening is seen over the SE source, where the color (1.1–2.2 $\mu$m) is 3.86 mag, and in a nearly complete ring surrounding the bright W source, where the color is 3.31 mag. For a population of stars with ages of $\lesssim 10^7$ yr, typical colors are $J - H = -0.2$, $H - K \sim 0.0$ mag. For a standard extinction law (Rieke & Lebofsky 1985) and the young population colors, the derived visual extinctions are $A_V$ = 17 (W), 15 (S), 24 (SE), 18 (NE), and 13 (all) mag on the basis of the observed $H - K$ magnitudes given in Table 1. For an old population ($J - H \sim 0.74$, $H - K \sim 0.24$ mag), the visual extinctions are 13, 11, 20, 14, and 9 mag, respectively, similar to the 1″ resolution estimates obtained by Larkin et al. (1995) from Pa$\alpha$ and Br$\gamma$ line ratios. Considerably higher estimates were obtained by Sturm et al. (1996), and it is clear that there are undoubtedly areas in the nucleus from which virtually no radiation escapes, even at 2.2 $\mu$m.

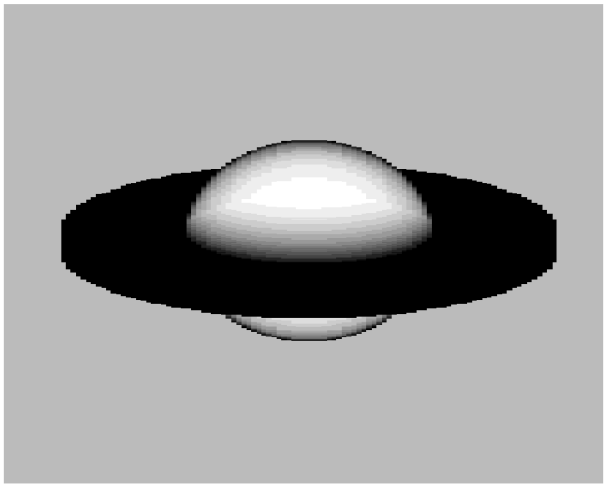

FIG. 6.—Galactic-nucleus star cluster with an embedded, opaque dust disk provides a possible explanation of the observed morphology in the Arp 220 W source (and possibly the NE-SE complex). In the model, the stellar density is constant out to the cutoff radius, and the disk is inclined 20° to the line of sight.

### 3.3. *Nuclear Structure*

The complex near-infrared structure of Arp 220 is due to their being multiple centers of star formation activity (as in Arp 299; cf. Wynn-Williams et al. 1991) and strongly varying dust obscuration within the merger nuclei. The relatively simple double-nuclei structure of the radio continuum (Baan & Haschick 1995) and the millimeter-wave dust continuum (Scoville et al. 1997) suggest that the major mass concentrations are associated with the W and SE sources. The NE and S sources would then be relatively minor mass concentrations, albeit with high present-epoch luminosity.

If the intrinsic, *unobscured* shapes of the expected stellar emission are either ellipsoidal (in the case of the nuclear core clusters), pointlike (for unresolved stellar clusters), or disklike (for young stars formed in disk), the unobscured morphology should appear spherical or elliptical depending on the viewing angle. For both the E and W nuclei, the morphology at 1.1–2.2 $\mu$m is clearly not elliptical: the western nucleus appears as a crescent, and the eastern nucleus is split into two components (NE and SE) with very different colors. Given our suggested registration of the radio and infrared, it is evident that the true centers of the nuclei are so obscured that neither is seen directly at 2.2 $\mu$m.

The crescent, or partial ring, morphology of the western component is clearest in the deconvolved 2.2 $\mu$m image (Fig. 4), but it is also apparent in the original 2.2 $\mu$m data (Fig. 2). This morphology might readily arise under two circumstances: if there is an obscuring disk of dust (and gas) embedded in the *spheroidal* nuclear star cluster or if a central starburst *ring* or disk of young stars is partially obscured by its own dust. Figure 6 models the surface brightness distribution for a star cluster in which the midplane is cut by a totally opaque dust disk; here, the observed crescent shape arises because of an increase in geometrical path length through the cluster periphery. The second hypothesis with a ring or torus of massive star formation

is similar to models proposed for Seyfert galaxy nuclei (e.g., Maolino & Rieke 1995; Genzel et al. 1995).

Two important characteristics of the observed emission should be emphasized: the crescent shape and the extremely abrupt cutoff by dust to the south of the W source. The former strongly implies that the dust is *embedded* in the core cluster/disk rather than being a foreground dust lane; the latter implies that the dust is in a extremely thin but very opaque disk. This geometry agrees with that suggested by Scoville et al. (1997) based on arcsecond resolution imaging of the millimeter CO line. The low velocity dispersion of the molecular gas implied a very thin disk ($\Delta z = 16$ pc). A similar disk structure in the nuclei has been suggested by Baan & Haschick (1995) on the basis of their $H_2CO$ data.

The morphology of the eastern nucleus is not so distinctive, yet the apparent bifurcation of the nucleus into lowly and highly reddened components (NE and SE, respectively) and the probable positioning of the radio nucleus in an area of weak 2.2 $\mu$m emission both suggest a nuclear dust disk—like that in the W nucleus. For both nuclei, the highest extinctions occur to the south of the radio centers, which suggests that the dust disks are tilted such that the south is the near side.

The measured infrared sizes (FWHM) of the W, SE, and NE source components are 0.″2–0.″5, corresponding to 75–185 pc. The separation of the radio nuclei (A and B) is 0.″98 or 364 pc in projection. Their actual separation is ~600 pc if the geometry suggested by Baan & Haschick (1995) and Scoville et al. (1997) is correct, since the nuclei would then be well off the major axis of their orbits. Within each of the nuclei, Scoville et al. (1997) detected CO emission profiles of full width of ~250 km s$^{-1}$. If the rotation velocities of gas within each nuclear cluster is ~125 km s$^{-1}$ at 75 pc radius, their dynamical masses are $\sim 3 \times 10^8\ M_\odot$.

### 3.4. *Unresolved Clusters*

Magnitudes and positions of eight clusters for which reliable measurements could be made are listed in Table 1 in order of decreasing flux at 1.1 $\mu$m. All of these sources are too bright to be individual stars. Given our resolution (~30 pc), the fact that they are unresolved is entirely consistent with their being globular clusters. Their measured offsets from the 2.2 $\mu$m centroid imply projected galactic radii of 0.9–2.7 kpc. The apparent clustering of these sources around Arp 220, with none seen beyond a 7.″5 radius, suggests that most of them must be associated with Arp 220 rather than being in the foreground. Given the fact that we have measured only two colors and must use one color to constrain the reddening, the remaining color does not strongly discriminate the ages of these clusters. The cluster sources outside a 2″ radius have measured colors at 1.1, 1.6, and 2.2 $\mu$m that are consistent (within the uncertainties) with those of globular clusters in NGC 5128 (Frogel 1984), which indicates that they could have ages of $\geq 10^9$ yr and essentially no near-infrared reddening ($A_V \leq 5$ mag). The absolute $K$ magnitude of the brightest cluster ($M_K = -13.5$ mag) in Arp 220 is ~1.5 mag brighter than the brightest cluster in NGC 5128 (Frogel 1984) and is comparable in brightness to the tip of the globular cluster luminosity function for ellipticals (Ajhar, Blakelee, & Tonry 1994).

The NICMOS project has been supported by NASA grant NAG 5-3042. It is a pleasure to acknowledge assistance and discussions of L. Armus, L. Bergeron, C. Boone, J. Goldader, A. Fruchter, J. Jensen, T. Soifer, J. Surace, and R. White. We are grateful to K. Borne and R. Lucas for sharing their *I*-band image of Arp 220 with us.

REFERENCES

Ajhar, E. A., Blakelee, J. P., & Tonry, J. L. 1994, AJ, 108, 2087
Armus, L., Shupe, D. L., Matthews, K., Soifer, B. T., & Neugebauer, G. 1995, ApJ, 440, 200
Baan, W. A., & Haschick, A. D. 1995, ApJ, 454, 745
Baan, W. A., van Gorkom, J. H., Schmelz, J. T., & Mirabel, I. F. 1987, ApJ, 313, 102
Borne, K., & Lucas, R. 1997, in preparation
Busko, I., & Stobie, E. 1997, preprint
Carico, D. P., Sanders, D. B., Soifer, B. T., Elias, J. H., Matthews, K., & Neugebauer, G. 1990, AJ, 95, 356
Frogel, J. 1984, ApJ, 278, 119
Genzel, R., Weitzel, L., Tacconi-Garman, L., Blietz, M., Cameron, M., Krabbe, A., Lutz, D., & Sternberg, A. 1995, ApJ, 444, 129
Graham, J. R., Carico, D. P., Matthews, K., Neugebauer, G., Soifer, B. T., & Wilson, T. D. 1990, ApJ, 354, L5
Joseph, R. D., & Wright, G. S. 1985, MNRAS, 214, 87
Maolino, R., & Rieke, G. H. 1995, ApJ, 454, 95
Larkin, J. E., Armus, L., Knop, R. A., Matthews, K., & Soifer, B. T. 1995, ApJ, 452, 599
Rieke, G. H., & Lebofsky, M. J. 1985, ApJ, 288, 618
Rieke, M. J., et al. 1997, in preparation
Scoville, N. Z., Yun, M. S., & Bryant, P. 1997, ApJ, 484, 702
Shaya, E., et al. 1994, AJ, 107, 1675
Shier, L. M., Rieke, M. J., & Rieke, G. H. 1996, ApJ, 470, 222
Soifer, B. T., Sanders, D. B., Madore, B. F., Neugebauer, G., Danielson, G. E., Elias, J. H., Lonsdale. C. J., & Rice, W. L. 1987, ApJ, 320, 74
Sturm, E., et al. 1996, A&A, 315, L133
Wynn-Williams, C. G., & Becklin, E. E. 1993, ApJ, 412, 535
Wynn-Williams, C. G., Eales, S. A., Becklin, E. E., Hodapp, K. W., Joseph, R. D., McLean, I. S., Simons, D. A., & Wright, G. S. 1991, ApJ, 377, 426

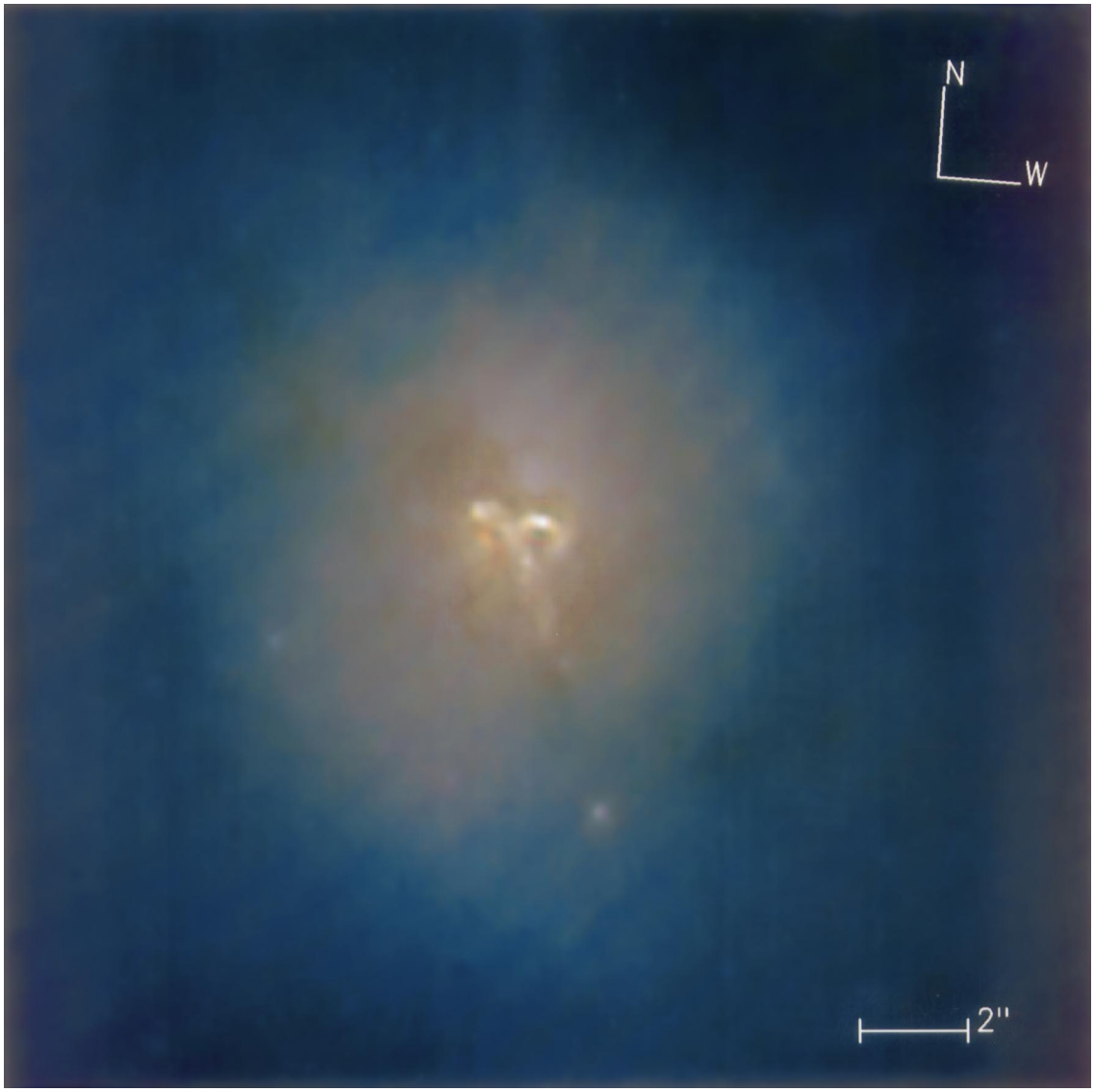


FIG. 1.—False color image of the 1.1, 1.6, and 2.22 $\mu$m data for the entire field of view (19″). The long-wavelength observations were deconvolved to 0.″14 resolution.

SCOVILLE et al. (see 492, L108)

PLATE L8

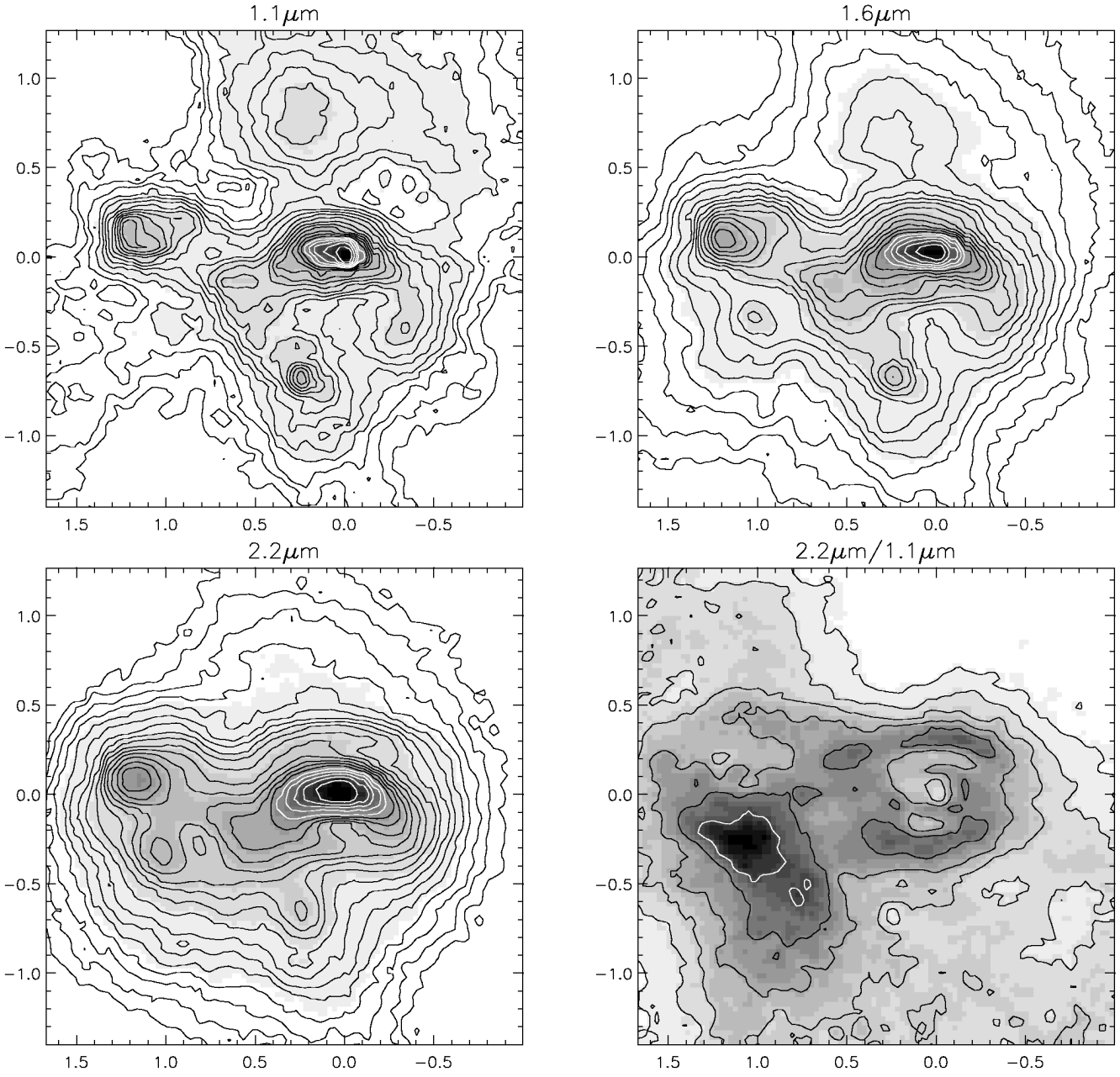


FIG. 2.—Contour and gray-scale images for the 1.1, 1.6, and 2.22 $\mu$m data for the central 2.″5 are shown together with the ratio 2.22/1.1 $\mu$m using the original resolution drizzled images. The coordinates are offsets in $\alpha$ and $\delta$ from the peak at 2.22 $\mu$m ($\alpha_{1950}$= 15$^h$32$^m$46.$^s$90, $\delta_{1950}$= +23°40′07.″94). The contours are spaced logarithmically by factors of 1.16, 1.17, and 1.16 down from the peak on the W source at 5.1, 15, and 20 mJy arcsec$^{-2}$ at 1.1, 1.6, and 2.22 $\mu$m. In the ratio map, the peak value is 15.8, and the contours are spaced by factors of 1.54.

SCOVILLE et al. (see 492, L108)

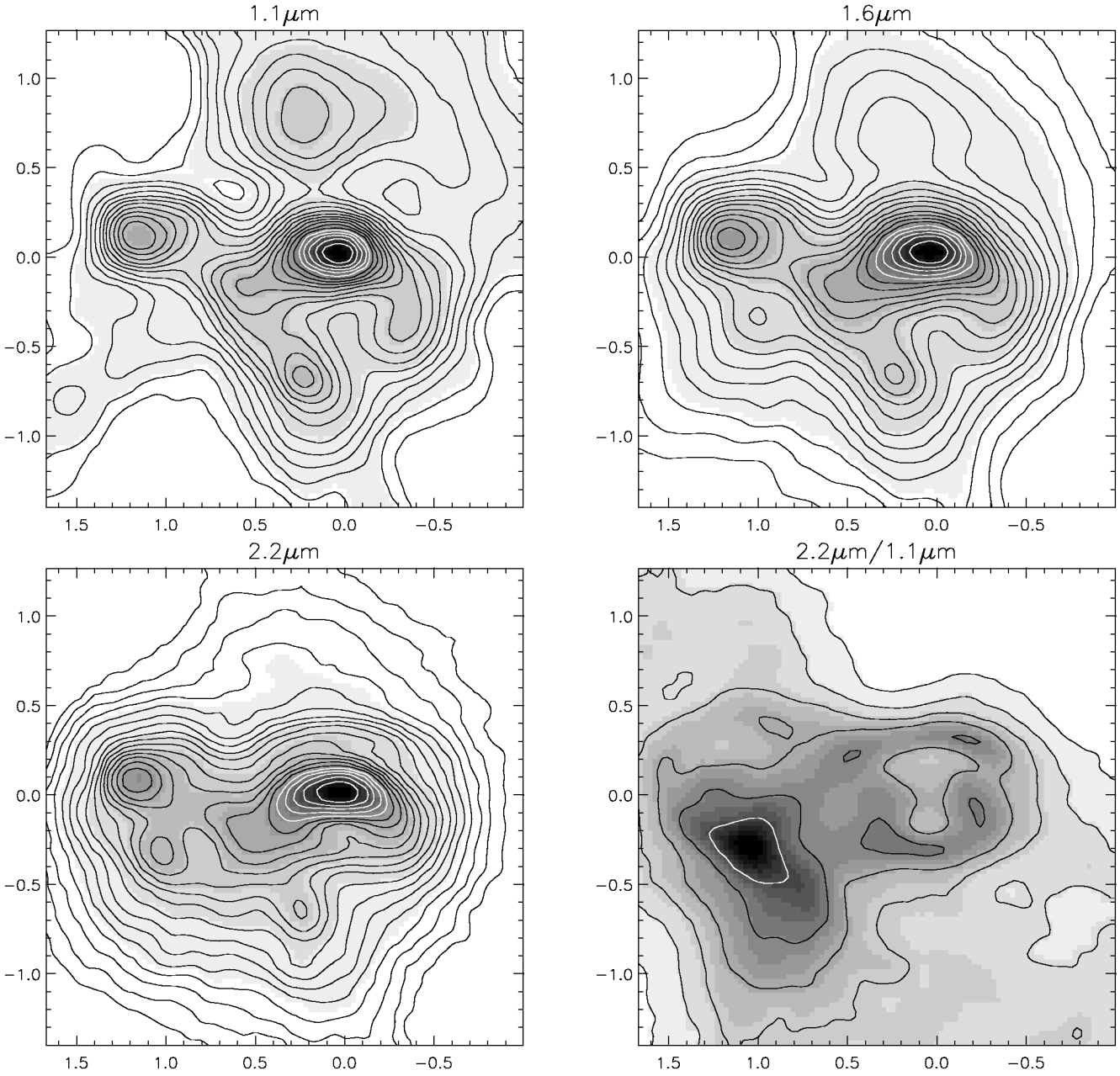


FIG. 3.—As in Fig. 2, except that the short-wavelength observations were convolved to a resolution of 0.″22 (i.e., the original resolution at 2.22 μm). The contours are spaced logarithmically by factors of 1.13, 1.14, and 1.16 down from the peak on the W source at 3.2, 11, and 19 mJy arcsec$^{-2}$ at 1.1, 1.6, and 2.22 μm. In the ratio map, the peak value is 15.2, and the contours are spaced by factors of 1.34.

SCOVILLE et al. (see 492, L108)

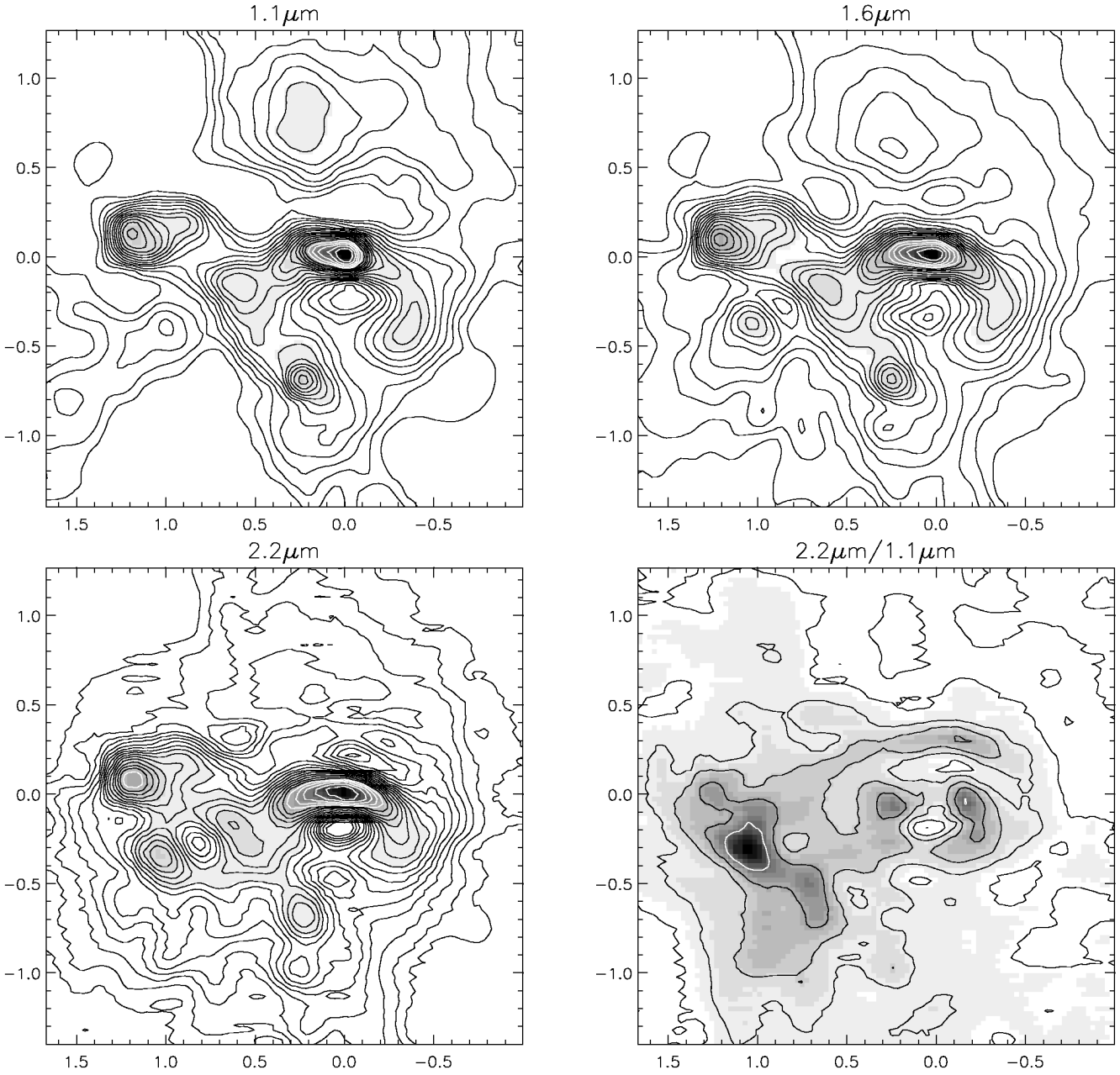


FIG. 4.—As in Fig. 2, except that the long-wavelength observations were deconvolved to 0.″14 resolution using Richardson-Lucy algorithm without damping. The contours are spaced logarithmically by factors of 1.21, 1.22, and 1.26 down from the peak on the W source. In the ratio map, the contours are spaced by factors of 1.65.